Banner appropriate to article type will appear here in typeset article

Water wave scattering by a surface-mounted rectangular anisotropic elastic plate

Ben Wilks^{1,2}, Michael H. Meylan¹, Zachary J. Wegert³, Vivien J. Challis³ and Ngamta Thamwattana¹

¹School of Information and Physical Sciences, University of Newcastle, Callaghan NSW 2308, Australia

(Received xx; revised xx; accepted xx)

Piezoelectric plates, which become electrically polarised in response to bending, have recently been proposed for water wave energy conversion. However, piezoelectric materials (e.g. Polyvinylidene Fluoride) can be anisotropic, which makes them challenging to model in three dimensions. This paper considers the simpler problem of water wave scattering by an anisotropic elastic plate, i.e., the piezoelectric effect is ignored. The problem is obtained as an expansion over the elastic plate modes. In turn, the component diffraction and radiation problems are solved by formulating a boundary integral equation and solving numerically using a constant panel method. The results are presented to highlight the resonant responses of the plate under different forcing scenarios. In particular, we illustrate how the excitation of certain modes can be forbidden due to symmetry. Although not considered in this paper, the method we present is applicable to piezoelectric plates, and thereby facilitates the extension of piezoelectric wave energy converter models to the three dimensional water wave setting.

Key words: Elastic waves; Wave scattering; Wave-structure interactions

1. Introduction

Hydroelasticity, which is concerned with the interaction of fluids with elastic bodies, is an important topic with numerous applications, including those in the cryosphere (ocean wave scattering by sea ice and ice shelves) and those related to the engineering of very large floating structures (VLFS). A comprehensive account of the historical research can be found in the review articles Squire (2007, 2020). We give here a brief account of some of the hydroelastic models. We note that this extensive research has focussed almost entirely on isotropic plates.

²UniSA STEM, The University of South Australia, Mawson Lakes SA 5095, Australia

³School of Mathematical Sciences, Queensland University of Technology, Brisbane QLD 4001, Australia **Corresponding author:** Ben Wilks, ben.wilks@unisa.edu.au

The two-dimensional water wave problem (one horizontal and one vertical) was solved by an eigenfunction expansion method by Fox & Squire (1994) and extended by Sahoo et al. (2001) who analysed a semi-infinite elastic plate floating on the surface of water of finite-depth. The Wiener-Hopf technique is particularly suited to semifinite problems and highly analytic solutions have been derived in this case (Balmforth & Craster 1999; Chung & Fox 2002; Tkacheva 2003; Williams & Meylan 2012; Smith et al. 2020). The finite elastic plate was solved by Meylan & Squire (1994) using Green's function technique, which led to a Fredholm integral equation and was simultaneously solved using a modal expansion by Newman (1994). The three-dimensional water wave problem involving circular elastic discs was solved by Meylan & Squire (1996); Peter et al. (2004). The solution for plates of arbitrary shapes was given in Meylan (2001, 2002). Similar methods were developed by Hermans (2004); Andrianov & Hermans (2006).

Recently, extensive studies on hydroelasticity have been driven by its potential applications in wave energy conversion, with flexible wave energy converters (WECs) continuing to be a focal point of current research (Babarit et al. 2017; Philen et al. 2018; Tay & Wei 2020; Collins et al. 2021; Renzi et al. 2021; Michele et al. 2022; Zheng et al. 2022; V. & Koley 2022; Guo et al. 2023; Singh & Gayen 2023; Cheng et al. 2024; Meylan et al. 2025). A promising mechanism for flexible wave energy conversion is the piezoelectric effect, in which materials become electrically polarised in response to elastic deformation. First comprehensively modelled by Renzi (2016), a piezoelectric WEC (usually modelled as a plate) would become polarised in response to deformation by ocean waves and thus induce a current in an external circuit. An important aspect of piezoelectric materials that has been hitherto ignored in the piezoelectric WEC literature is their anisotropy while piezoceramics are usually transversely isotropic (Yang 2018), the polymer PVDF, which is often proposed for piezoelectric WECs, are anisotropic (Vinogradov & Holloway 1999). To date, authors have bypassed considerations of anisotropy by focusing on the one-dimensional WEC/two-dimensional fluid context, with submerged horizontal plates (Renzi 2016; V. & Koley 2022), surface mounted plates (Meylan et al. 2025) and vertical plates (Singh & Gayen 2023) being among the cases considered. The present paper seeks to investigate wave scattering by a two-dimensional anisotropic elastic plate in a threedimensional fluid. In doing so, this paper will facilitate future extensions of earlier models of piezoelectric WECs (Renzi 2016; Meylan et al. 2025) to three dimensions.

The outline of this paper is as follows. In §2 we describe a model of a rectangular anisotropic elastic plate mounted on the water surface. Our method is an extension of that presented by Meylan *et al.* (2025) for the two-dimensional case, in which the solution is expanded as a sum of a diffraction potential and a superposition of radiation potentials. The diffraction potential, which assumes that the plate is fixed, is solved in §3. The modes of vibration of the plate and the corresponding radiation potentials are found in §4 and §5, respectively. The coupled fluid/plate problem is solved in §6. An energy balance identity used to verify our computations, which is based on the optical theorem, is derived in §7. The results are presented in §8 in order to illustrate the capabilities of the model. The conclusion is given in §9.

2. Problem outline

2.1. Preliminaries

We consider the scattering of water waves by a rectangular anisotropic elastic plate situated at the surface of the water and having negligible draft. We adopt a three-dimensional Cartesian coordinate system (x, y, z) for the fluid domain, where x and y are horizontal coordinates parallel to the plate edges, and the z coordinate points vertically upward (i.e., it

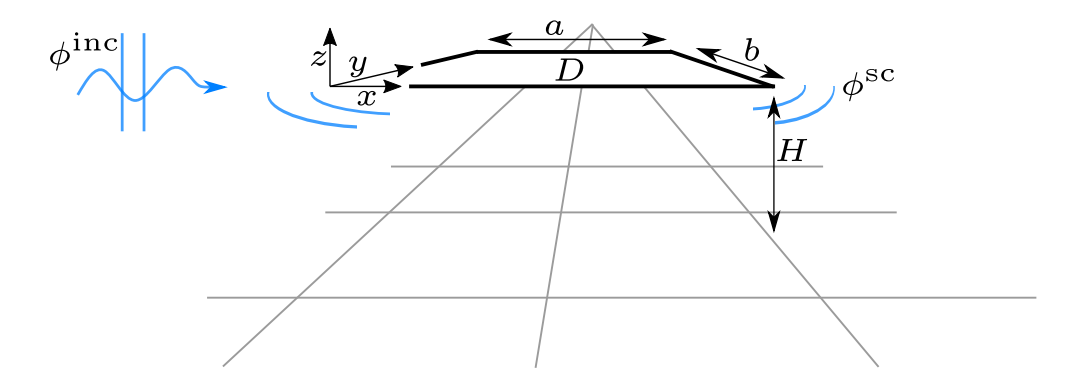


Figure 1. Perspective diagram of the surface-mounted rectangular plate scattering problem. The rectangular plate, labelled D, has side lengths a and b. The flat seabed is drawn using grey lines. The incident wave $\phi^{\rm inc}$ excites the plate into motion, generating scattered waves $\phi^{\rm sc}$.

is normal to the plate at rest). At equilibrium, the fluid occupies the region $\Omega = \mathbb{R}^2 \times (-H, 0)$, where H is the depth of the fluid, and the plate occupies the region $D \times \{0\}$, where $D = (0, a) \times (0, b)$. A schematic of the geometry is shown in Figure 1.

The fluid is assumed to be incompressible, irrotational and inviscid, meaning that the time dependent velocity potential Φ satisfies

$$\Delta \Phi = 0 \quad \forall (x, y, z) \in \Omega, \tag{2.1}$$

where $\Phi = \Phi(x, y, z, t)$ and $\Delta = \partial_x^2 + \partial_y^2 + \partial_z^2$. The velocity of the fluid is given by $\mathbf{v} = \nabla \Phi$. There is no flow normal to the seabed at z = -H, which implies

$$\partial_z \Phi = 0 \quad z = -H, (x, y) \in \mathbb{R}^2.$$
 (2.2)

The free surface of the fluid occupies the region $(x, y) \in \mathbb{R}^2 \setminus D$. The free surface of the fluid is governed by the kinematic and dynamic boundary conditions, which are

$$\partial_t \zeta = \partial_z \Phi \bigg|_{z=0},\tag{2.3a}$$

$$\zeta = -\frac{1}{g} \partial_t \Phi \bigg|_{z=0},\tag{2.3b}$$

respectively, where $\zeta = \zeta(x, y, t)$ is the displacement of the free surface of the fluid from equilibrium and g is the acceleration due to gravity.

The plate, which has uniform thickness h, is assumed to be thin, which means $a, b \gg h$. The motion of the plate is modelled using Kirchoff–Love theory, which gives rise to an equation of the form

$$\rho h \partial_t^2 W + \mathcal{P} W = Q, \tag{2.4}$$

where W(x, y, t) is the vertical displacement of the plate and ρ is the density of the plate. The fourth order differential operator \mathcal{P} is given by

$$\mathcal{P} = D_{11}\partial_x^4 + 4D_{16}\partial_x^3\partial_y + 2(D_{12} + 2D_{66})\partial_x^2\partial_y^2 + 4D_{26}\partial_x\partial_y^3 + D_{22}\partial_y^4, \tag{2.5}$$

where D_{ij} are the bending and twisting rigidities. Note that in the isotropic case, $D_{11} = D_{22} = D_{12} + 2D_{66} > 0$ and $D_{16} = D_{26} = 0$, in which case \mathcal{P} is proportional to the biharmonic operator. The applied load Q, which has units of force per area, is taken to be

positive when the load is directed upward. The plate is assumed to be clamped on all sides, which yields the boundary conditions

$$W(0, y) = W(a, y) = \partial_x W(0, y) = \partial_x W(a, y) = 0,$$
 (2.6a)

$$W(x,0) = W(x,b) = \partial_{y}W(x,0) = \partial_{y}W(x,b) = 0.$$
 (2.6b)

More generally, other linear homogeneous boundary conditions, such as those describing simply supported or free edges (or combinations thereof) can be considered within our formulation. We do not explore these cases here for ease of presentation.

The motions of the fluid and the plate are coupled through kinematic and dynamic boundary conditions. The kinematic condition, which equates the fluid velocity at the plate interface with the plate velocity, is

$$\partial_z \Phi \bigg|_{z=0} = \partial_t W, \tag{2.7}$$

for $(x, y) \in D$. The applied load acting on the plate is due to the pressure of the fluid at the interface of the plate. As the hydrostatic and hydrodynamic pressure in the fluid is given by

$$P_{\text{hydrostatic}} = -\rho_w gz \quad \text{and} \quad P_{\text{dynamic}} = -\rho_w \partial_t \Phi,$$
 (2.8)

respectively, in which ρ_w is the fluid density, the dynamic condition on the plate becomes

$$\rho h \partial_t^2 W + \mathcal{P} W = -\rho_w g W - \rho_w \partial_t \Phi \bigg|_{z=0}. \tag{2.9}$$

2.2. Time harmonic formulation

We assume a time harmonic motion with angular frequency ω , which implies that we can write

$$\Phi(x, y, z, t) = \operatorname{Re}\{\phi(x, y, z)e^{-i\omega t}\} \qquad (x, y, z) \in \Omega,$$
(2.10a)

$$\zeta(x, y, t) = \operatorname{Re}\{\eta(x, y)e^{-i\omega t}\} \qquad (x, y) \in \mathbb{R}^2 \setminus D, \qquad (2.10b)$$

$$W(x, y, t) = \text{Re}\{w(x, y)e^{-i\omega t}\}\$$
 $(x, y) \in D.$ (2.10c)

This leads to the following boundary value problem for ϕ :

$$\Delta \phi = 0 \qquad (x, y, z) \in \Omega, \qquad (2.11a)$$

$$\partial_z \phi = 0$$
 $z = -H, \quad (x, y) \in \mathbb{R}^2,$ (2.11b)

$$\partial_z \phi = \alpha \phi$$
 $z = 0, \quad (x, y) \in \mathbb{R}^2 \setminus D,$ (2.11c)

$$\partial_z \phi = -i\omega w$$
 $z = 0, \quad (x, y) \in D,$ (2.11d)

$$\sqrt{r}(\partial_r - ik)(\phi - \phi^{inc}) \to 0$$
 as $r \to \infty$, (2.11e)

with $\alpha = \omega^2/g$, which must be solved in tandem with the plate equation

$$\mathcal{P}\mathbf{w} - \omega^2 \rho h \mathbf{w} + \rho_w g \mathbf{w} = i\omega \rho_w \phi \bigg|_{z=0}, \qquad (2.11f)$$

for $(x, y) \in D$, where the plate satisfies the clamped boundary conditions (2.6). In the Sommerfeld condition (2.11e), $r = \sqrt{x^2 + y^2}$ and k is the positive real root of the dispersion relation

$$k \tanh(kH) = \alpha. \tag{2.12}$$

3. Diffraction by a rigid plate

We first consider the diffraction potential ϕ^{di} , which describes the scattering of a prescribed incident wave ϕ^{in} by a plate held fixed in a flat configuration at the fluid surface. This potential satisfies the boundary value problem consisting of (2.11a), (2.11b), (2.11c), (2.11e), together with the no flow condition on the plate

$$\partial_z [\phi^{\text{in}} + \phi^{\text{di}}] = 0 \quad \text{for } z = 0, \quad (x, y) \in D.$$
 (3.1)

The unknown diffraction potential is obtained by solving a boundary integral equation.

3.1. Green's function

The Green's function for a three-dimensional fluid of constant depth satisfies

$$\Delta G = \delta(x)\delta(y)\delta(z - z') \qquad (x, y, z) \in \Omega, \tag{3.2a}$$

$$\partial_z G = \alpha G$$
 $z = 0,$ (3.2b)
 $\partial_z G = 0$ $z = 0,$ (3.2c)

$$\partial_z G = 0 z = 0, (3.2c)$$

$$\sqrt{r}(\partial_r G - ikG) \to 0$$
 as $z \to \infty$, (3.2d)

where $\delta(x)$ is the Dirac delta and (0,0,z') is the location of the source. For z=z'=0, the Green's function has the following representation (Linton & McIver 2001)

$$-4\pi G(r) = \frac{1}{r} + \frac{1}{\sqrt{r^2 + 4H^2}} + \int_0^\infty \frac{2(\mu + \alpha)e^{-\mu H}\cosh^2\mu H}{\mu\sinh\mu H - \alpha\cosh\mu H} J_0(\mu r) d\mu, \tag{3.3}$$

where J_0 is the zeroth order Bessel function of the first kind and f denotes complex contour integration beneath any poles on the real line. To evaluate the above integral numerically, we first write $J_0(x) = \frac{1}{2}(H_0^{(1)}(x) + H_0^{(2)}(x))$ (where $H_0^{(1)}$ and $H_0^{(2)}$ are the zeroth order Hankel functions of the first and second kind, respectively) and deform the contour of integration using residue calculus. We obtain the following rapidly converging representation of the Green's function:

$$-4\pi G(r) = \frac{1}{r} + \frac{1}{\sqrt{r^2 + 4H^2}} + 2\text{Re}\left\{ \int_C \frac{(\mu + \alpha)e^{-\mu H}\cosh^2\mu H}{\mu\sinh\mu H - \alpha\cosh\mu H} H_0^{(1)}(\mu r) d\mu \right\} + \frac{i\pi}{HM^2}\cosh^2(kH) H_0^{(1)}(kr),$$
(3.4)

where C is parametrised by $e^{i\pi/4}t$ for $0 \le t < \infty$ and

$$M^2 = \frac{1}{2} \left(1 + \frac{\sinh 2kH}{2kH} \right).$$

The integral in (3.4) is calculated using the MATLAB routine integral.

3.2. Integral equation for diffraction problem

Let B_R be the cylinder of points satisfying -H < z < 0 and $x^2 + y^2 < R^2$. Since ϕ^{di} is harmonic, an application of Green's third identity gives

$$\phi^{\mathrm{di}}(\mathbf{x}) = \int_{\partial B_R} \phi^{\mathrm{di}}(\mathbf{x}') \partial_{n'} G(\mathbf{x}', \mathbf{x}) - G(\mathbf{x}', \mathbf{x}) \partial_{n'} \phi^{\mathrm{di}}(\mathbf{x}') \mathrm{d}S_{\mathbf{x}'}, \tag{3.5}$$

where, in abuse of notation, $G(\mathbf{x}', \mathbf{x})$ denotes the value of the Green's function at the point $\mathbf{x} = (x, y, z)$ for a source located at $\mathbf{x}' = (x', y', z')$, whenever its arguments are bold. In

(3.5), $\partial_{n'}$ the derivative in the direction of the outwards-pointing unit normal at \mathbf{x}' . As $R \to \infty$, the boundary conditions in (3.2) and those governing the diffraction problem reduce (3.5) to

$$\phi^{\mathrm{di}}(\mathbf{x}) = \alpha \int_{D \times \{0\}} G(\mathbf{x}', \mathbf{x}) (\phi^{\mathrm{in}}(\mathbf{x}') + \phi^{\mathrm{di}}(\mathbf{x}')) \mathrm{d}S_{\mathbf{x}'}. \tag{3.6}$$

An integral equation is obtained from the above by restricting $\mathbf{x} = (x, y, z) \in D \times \{0\}$, namely,

$$\phi^{\text{di}}(x, y, 0) = \alpha \iint_D G(\sqrt{(x - x')^2 + (y - y')^2}, 0) \left(\phi^{\text{in}}(x', y', 0) + \phi^{\text{di}}(x', y', 0)\right) dx' dy',$$
(3.7)

for all $(x, y) \in D$.

3.3. Numerical solution using a constant panel method

The boundary integral equation above is solved using a constant panel method. To do so, we discretise the plate region D into a grid of $N_x \times N_y$ squares \Box_j . Each square has dimensions $\Delta x \times \Delta x$ and midpoints (x_j, y_j) . Evaluated at nodes (x_i, y_i) , equation (3.7) becomes

$$\phi^{\text{di}}(x_{i}, y_{i}, 0) = \alpha \sum_{j=1}^{N_{x} \times N_{y}} \iint_{\square_{j}} G(\sqrt{(x_{i} - x')^{2} + (y_{i} - y')^{2}}, 0) \left(\phi^{\text{in}}(x', y', 0) + \phi^{\text{di}}(x', y', 0)\right) dx' dy'$$

$$\approx \alpha \sum_{j=1}^{N_{x} \times N_{y}} \left(\phi^{\text{in}}(x_{j}, y_{j}, 0) + \phi^{\text{di}}(x_{j}, y_{j}, 0)\right) \iint_{\square_{j}} G(\sqrt{(x_{i} - x')^{2} + (y_{i} - y')^{2}}, 0) dx' dy',$$

$$(3.8b)$$

where (3.8*b*) is the constant panel assumption, valid when ϕ^{in} and ϕ^{di} are slowly varying relative to the grid spacing. Letting $(\phi^{\text{di}})_j = \phi^{\text{di}}(x_j, y_j, 0)$ and $(\phi^{\text{in}})_j = \phi^{\text{in}}(x_j, y_j, 0)$, Equation (3.8*b*) may be recast in matrix form as

$$(I - \alpha K)(\phi^{\text{in}} + \phi^{\text{di}}) = \phi^{\text{in}}, \tag{3.9}$$

to be solved for ϕ^{di} , where *I* is the $(N_x \times N_y)$ -dimensional identity matrix. The entries in the kernel matrix *K* are chosen to approximate the integrals over the squares \Box_j appearing in (3.8*b*), namely,

$$(K)_{ij} \approx \iint_{\square_i} G(\sqrt{(x_i - x')^2 + (y_i - y')^2}, 0) dx' dy'.$$
 (3.10)

We approximate the off diagonal entries of K as

$$(K)_{ij} = G\left(\sqrt{(x_i - x_j)^2 + (y_i - y_j)^2}, 0\right) \Delta x^2,$$
(3.11)

for $i \neq j$. This is equivalent to midpoint quadrature on the grid. For diagonal entries, we use the constant panel assumption to write

$$(K)_{jj} = \iint_{\square_j} G\left(\sqrt{(x - x_j)^2 + (y - y_j)^2}, 0\right) dxdy$$
 (3.12a)

$$= \int_{-\Delta x/2}^{\Delta x/2} \int_{-\Delta x/2}^{\Delta x/2} G\left(\sqrt{x^2 + y^2}, 0\right) dx dy, \tag{3.12b}$$

for all j, where the second line follows from translation. The double integral is then calculated by (i) directly integrating the term 1/r in (3.4), and (ii) using the MATLAB routine integral2 to integrate the remaining part. Our numerical code for the diffraction problem was validated for the case of a circular plate, using a code developed to solve the problem of wave scattering by a partially submerged truncated circular cylinder, which is valid in the limit of negligible submergence (Wilks *et al.* 2025). The aforementioned code uses separation of variables in cylindrical coordinates to solve the problem both beneath and exterior to the plate. Subsequently, continuity conditions between the interior and exterior regions reduce to integral equations that are solved numerically using a singularity respecting Galerkin method.

4. Modes of vibration of the plate

The modes of vibration of the plate are the eigenfunctions w_j of the operator \mathcal{P} , which satisfy

$$\mathcal{P}\mathbf{w}_j = \rho h \omega_j^2 \mathbf{w}_j, \tag{4.1}$$

where ω_j are the angular frequencies of the vibrational modes. Each mode can be written as

$$\mathbf{w}_{j}(x,y) = \sum_{m=1}^{\infty} \sum_{n=1}^{\infty} \frac{A_{mn}^{(j)}}{\kappa_{m}^{4} \kappa_{n}^{4}} u_{m} \left(\frac{x}{a}\right) u_{n} \left(\frac{y}{b}\right), \tag{4.2}$$

where u_m and κ_m^4 are the eigenfunctions and eigenvalues of the fourth order differential operator on the unit interval with clamped boundary conditions. The eigenfunctions are equivalently the modes of vibration of an Euler–Bernoulli beam. The modes satisfy

$$\partial_x^4 u = \kappa^4 u, \tag{4.3a}$$

$$u(0) = u(1) = 0, (4.3b)$$

$$\partial_x u(0) = \partial_x u(1) = 0. (4.3c)$$

These modes are normalised so that

$$\int_0^1 u_m(x)u_n(x)\mathrm{d}x = \delta_{mn},\tag{4.4}$$

where δ_{mn} is the Kronecker delta. Further details about these eigenmodes are given in Appendix A. Note that (4.2) automatically satisfies the clamped boundary conditions at

the plate edges (2.6). Substitution of (4.2) into (4.1) gives

$$\sum_{m=1}^{\infty} \sum_{n=1}^{\infty} A_{mn}^{(j)} \left[\frac{D_{11}}{\kappa_n^4 a^4} u_m \left(\frac{x}{a} \right) u_n \left(\frac{y}{b} \right) + \frac{4D_{16}}{\kappa_m^4 \kappa_n^4 a^3 b} u_m''' \left(\frac{x}{a} \right) u_n' \left(\frac{y}{b} \right) \right. \\ + \frac{2(D_{12} + 2D_{66})}{\kappa_m^4 \kappa_n^4 a^2 b^2} u_m'' \left(\frac{x}{a} \right) u_n'' \left(\frac{y}{b} \right) \\ + \frac{4D_{26}}{\kappa_m^4 \kappa_n^4 a b^3} u_m' \left(\frac{x}{a} \right) u_n''' \left(\frac{y}{b} \right) + \frac{D_{22}}{\kappa_m^4 b^4} u_m \left(\frac{x}{a} \right) u_n \left(\frac{y}{b} \right) \right] \\ = \omega_j^2 \rho h \sum_{m=1}^{\infty} \sum_{n=1}^{\infty} \frac{A_{mn}^{(j)}}{\kappa_m^4 \kappa_n^4} u_m \left(\frac{x}{a} \right) u_n \left(\frac{y}{b} \right), \tag{4.5}$$

where we have used the fact that $u_m^{(4)} = \kappa_m^4 u_m$. Next, we seek a Galerkin approximation, by first truncating each of the series in (4.5) after N_{beam} terms, then assuming that the residual is orthogonal to the basis functions $u_p(x/a)u_q(y/b)$ for $1 \le p, q \le N_{\text{beam}}$. These steps yield

$$\left(\frac{D_{11}}{\kappa_{q}^{4}a^{4}} + \frac{D_{22}}{\kappa_{p}^{4}b^{4}}\right)A_{pq}^{(j)} + \sum_{m=1}^{N_{\text{beam}}} \sum_{n=1}^{N_{\text{beam}}} \left(\frac{4D_{16}}{\kappa_{n}^{3}a^{3}\kappa_{m}b} \mathcal{U}_{mp}^{[3]} \mathcal{U}_{nq}^{[1]} + \frac{2(D_{12} + 2D_{66})}{\kappa_{n}^{2}a^{2}\kappa_{m}^{2}b^{2}} \mathcal{U}_{mp}^{[2]} \mathcal{U}_{nq}^{[2]} + \frac{4D_{26}}{\kappa_{n}a\kappa_{m}^{3}b^{3}} \mathcal{U}_{mp}^{[1]} \mathcal{U}_{nq}^{[3]}\right) A_{mn}^{(j)} \approx \omega_{j}^{2} \frac{\rho h}{\kappa_{p}^{4}\kappa_{q}^{4}} A_{pq}^{(j)}, \quad (4.6)$$

for $1 \le p, q \le N_{\text{beam}}$, where we have defined

$$\mathcal{U}_{mp}^{[l]} = \frac{1}{k_m^l} \int_0^1 u_m^{(l)}(x) u_p(x) dx, \tag{4.7}$$

for $l \in \{1, 2, 3\}$, where $u_m^{(l)}$ denotes the *l*th derivative of u_m . Equation (4.6) is a generalised eigenvalue problem of dimension N_{beam}^2 for the coefficients $A_{mn}^{(j)}$, which we solve numerically. The eigenmodes $w_j(x, y)$, which are recovered from these coefficients using (4.2), are normalised so that

$$\int_{0}^{a} \int_{0}^{b} \mathbf{w}_{m}(x, y) \mathbf{w}_{n}^{*}(x, y) dy dx = \delta_{mn}, \tag{4.8}$$

where the asterix denotes the conjugate transpose. We take $N_{\rm beam}=20$ throughout this paper. We have validated our method for computing the vibration modes using results provided by Leissa (1973) in the case where the plate is isotropic, and results provided in An *et al.* (2021) in the case where the plate is anisotropic, with excellent agreement—see the first and third rows of Figure 2.

5. Radiation potentials

For each vibration mode of the plate w_j , we compute the radiation potential $\phi_j^{\rm ra}$, namely the velocity potential of the fluid induced by the plate motion in the form $w = \text{Re}\{w_j(x,y)e^{-i\omega t}\}$. The radiation potential $\phi_j^{\rm ra}$ satisfies the boundary value problem consisting of (2.11*a*), (2.11*b*), (2.11*c*), (2.11*e*) and the kinematic condition

$$\partial_z \phi_i^{\text{ra}} = -i\omega w_j. \tag{5.1}$$

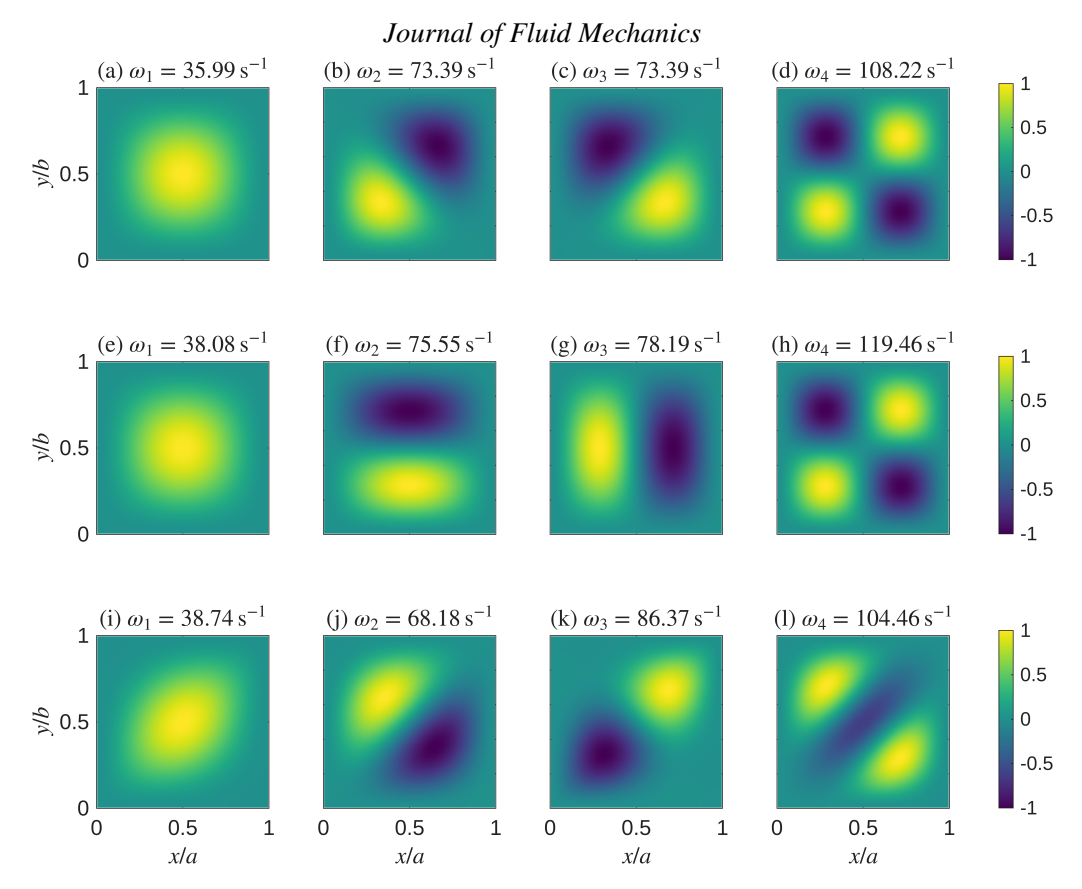


Figure 2. First four mode shapes of a square (a–d) isotropic plate (e–h) orthotropic plate and (i–l) anisotropic plate. The rigidity coefficients associated with these terms are given in Table 1. The remaining parameters are a = b = 1 m and $\rho h = 1$ kg m⁻¹. Note the mode shapes have been rescaled as $w_j(x, y)/p_j$, with p_j chosen for presentation.

	Isotropic	Orthotropic	Anisotropic
D_{11}	1 1 0.5 0 0 0.25	1	1
D_{22}	1	0.8750	1
D_{12}	0.5	0.3958	0.9082
D_{16}	0	0	0.6724
D_{26}	0	0	0.6724
D_{66}	0.25	0.6896	0.9341

Table 1. Rigidity coefficients used to generate the results in this paper. The coefficients for the anisotropic plate are as in An *et al.* (2021). All units are in Pa m⁴.

Following the steps outlined in §3.2, we use Green's third identity to compute

$$\phi_j^{\text{ra}}(\mathbf{x}) = \int_{D \times \{0\}} \phi_j^{\text{ra}}(\mathbf{x}') \partial_{n'} G(\mathbf{x}', \mathbf{x}) - G(\mathbf{x}', \mathbf{x}) \partial_{n'} \phi_j^{\text{ra}}(\mathbf{x}') dS_{\mathbf{x}'}.$$
 (5.2)

An application of (5.1) and (3.2b) reduces the above to

$$\phi_j^{\text{ra}}(\mathbf{x}) = \int_{D \times \{0\}} G(\mathbf{x}', \mathbf{x}) (\alpha \phi_j^{\text{ra}}(\mathbf{x}') + i\omega \mathbf{w}_j(\mathbf{x}')) dS_{\mathbf{x}'}.$$
 (5.3)

Applying the constant panel discretisation method used in (3.3) then yields the matrix equation

$$(I - \alpha K) \left(\phi_j^{\text{ra}} + \frac{ig}{\omega} \mathbf{w}_j \right) = \frac{ig}{\omega} \mathbf{w}_j, \tag{5.4}$$

to be solved for ϕ_j^{ra} , where $(\phi_j^{\text{ra}})_i = \phi_j^{\text{ra}}(x_i, y_i)$ and $(\mathbf{w}_j)_i = \mathbf{w}_j(x_i, y_i)$.

6. Scattering by an elastic plate

The solution to the coupled fluid-plate system of equations (2.11) is obtained by expanding in the modes of vibration of the plate. That is, the total potential is taken to be a superposition of the incident potential, the diffraction potential plus a weighted sum of the radiation potentials

$$\phi = \phi^{\text{in}} + \phi^{\text{di}} + \sum_{i=1}^{\infty} c_j \phi_j^{\text{ra}}, \tag{6.1}$$

where the coefficients c_j are unknown. By the kinematic condition (2.11*d*), the deformation of the plate is of the form

$$\mathbf{w} = \sum_{i=1}^{\infty} c_i \mathbf{w}_i. \tag{6.2}$$

The dynamic condition (2.11f), when multiplied by w_m^* and integrated over the plate, then yields

$$\rho h \omega_m^2 c_m - \rho h \omega^2 c_m + \rho_w g c_m = i \omega \rho_w \int_{D \times \{0\}} \phi w_m^* dS, \qquad (6.3)$$

where we have used (4.1). Substituting (6.1) into the above then yields

$$\rho h \omega_m^2 c_m - \rho h \omega^2 c_m + \rho_w g c_m - \mathrm{i} \omega \rho_w \sum_{j=1}^{\infty} \left(\int_{D \times \{0\}} \phi_j^{\mathrm{ra}} \mathbf{w}_m^* \mathrm{d} S \right) c_j = \mathrm{i} \omega \rho_w \int_{D \times \{0\}} (\phi^{\mathrm{in}} + \phi^{\mathrm{di}}) \mathbf{w}_m^* \mathrm{d} S.$$

$$(6.4)$$

Numerical evaluation of the integrals in the above, and truncation of the series after N terms, yields an $N \times N$ system for the unknown coefficients c_1, \ldots, c_N . Equation (6.4) becomes

$$(K - \omega^2 M + C - \omega^2 A - i\omega B)\mathbf{c} = \mathbf{f},$$
(6.5)

where *K*, *M* and *C* are the stiffness, mass and hydrostatic restoration matrices of the system, respectively, given by

$$K = \rho h \operatorname{diag}(\omega_m^2), \tag{6.6a}$$

$$M = -\rho hI, (6.6b)$$

$$C = \rho_w g I, \tag{6.6c}$$

where I is the $N \times N$ identity matrix. Moreover, the real-valued added mass and damping matrices A and B, respectively, are such that

$$-\omega^2 A_{mj} - i\omega B_{mj} = -i\omega \rho_w \int_{D\times\{0\}} \phi_j^{\text{ra}} w_m^* dS, \qquad (6.6d)$$

the vector of unknown coefficients is $\mathbf{c} = [c_1, \dots, c_N]^{\mathsf{T}}$, and the forcing vector is

$$(\mathbf{f})_m = \mathrm{i}\omega \rho_w \int_{D\times\{0\}} (\phi^{\mathrm{in}} + \phi^{\mathrm{di}}) \mathbf{w}_m^* \mathrm{d}S. \tag{6.6e}$$

Note that in this paper N=30 plate modes were considered, which was considered sufficient based on the energy balance validation in the following section.

7. Energy balance calculations

To verify our calculations, an energy balance identity is derived for the case in which the plate is excited by an incident plane wave of amplitude A and incident angle χ , namely

$$\phi^{\text{in}}(x, y, z) = \frac{-igA}{\omega} \frac{\cosh(k(z+H))}{\cosh(kH)} e^{ik(x\cos\chi + y\sin\chi)},$$
(7.1)

such that the corresponding free surface elevation is $\eta^{\text{in}}(x, y) = e^{ikx}$. Let (r, θ, z) be the system of cylindrical coordinates with $x = r \cos \theta$ and $y = r \sin \theta$. For large r, the potential can be approximated as (Mei *et al.* 2005)

$$\phi \sim \frac{-igA}{\omega} \frac{\cosh(k(z+H))}{\cosh(kH)} \left(e^{ikr\cos(\theta-\chi)} + \sqrt{\frac{2}{\pi kr}} f(\theta) e^{i(kr-\pi/4)} \right). \tag{7.2}$$

In the above, the first term in the brackets describes the incident wave and the second term describes the scattered wave. Thus, the far field pattern f must be derived from the scattered field. We first note that the total scattered field is of the form

$$\phi - \phi^{\text{in}} = \int_{D \times \{0\}} G(\mathbf{x}', \mathbf{x}) u(\mathbf{x}') dS_{\mathbf{x}'}, \tag{7.3}$$

where, with reference to (3.6) and (5.3),

$$u(x,y) = \alpha(\phi^{\text{in}}(x,y,0) + \phi^{\text{di}}(x,y,0)) + \sum_{j=1}^{\infty} c_j(\alpha\phi_j^{\text{ra}}(x,y,0) + i\omega w_j(x,y)).$$
 (7.4)

Asymptotically, the Green's function for a source at (x, y, z) = (0, 0, 0) is (Linton & McIver 2001)

$$G(r,\theta,z;0,0) \sim -\frac{\mathrm{i}}{2} \frac{k \cosh(k(z+H))}{k H \operatorname{sech}(kH) + \sinh(kH)} \sqrt{\frac{2}{\pi k r}} e^{\mathrm{i}(kr-\pi/4)}. \tag{7.5}$$

Suppose the source point of the Green's function is shifted to (x', y', 0). Let d(x', y') and $\alpha(x', y')$, respectively, be the radial and angular coordinates of the point (x', y', 0) with respect to the global origin (0, 0, 0). Then as $r \to \infty$, the Green's function is asymptotically (Falnes 2002)

$$G(r, \theta, z; x', y') \sim -\frac{i}{2} \frac{k \cosh(k(z+H))}{k H \operatorname{sech}(kH) + \sinh(kH)} \sqrt{\frac{2}{\pi k r}} \times \exp(i(kr - kd(x', y') \cos(\alpha(x', y') - \theta) - \pi/4)).$$
(7.6)

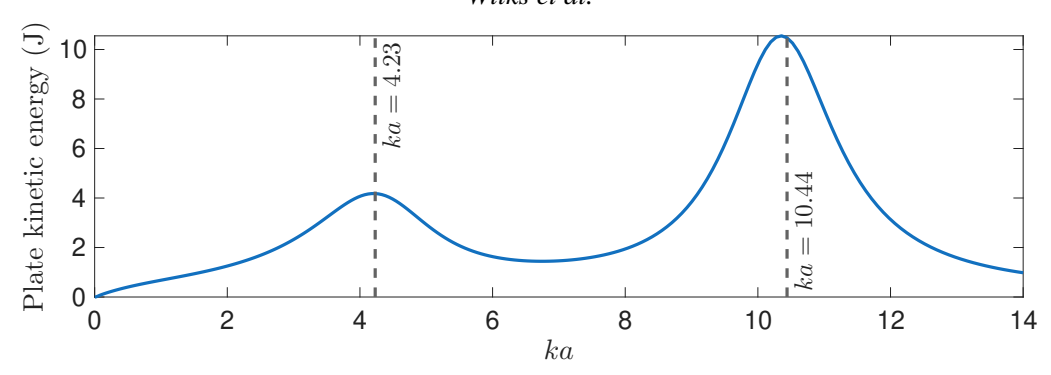


Figure 3. Kinetic energy spectrum for a square isotropic plate, with a = b = 1 m.

With reference to (7.2), substitution of the above expression into (7.3) eventually yields

$$f(\theta) = \frac{k\omega}{2g[kH\operatorname{sech}^{2}(kH) + \tanh(kH)]} \iint_{D} u(x', y') e^{-ikd(x', y')\cos(\alpha(x', y') - \theta)} dy' dx'.$$
(7.7)

Conservation of energy implies that the optical theorem holds, which is (Mei et al. 2005)

$$\frac{1}{2\pi} \int_{-\pi}^{\pi} |f(\theta)|^2 d\theta = -\text{Re}\{f(\chi)\}. \tag{7.8}$$

We have used this identity to verify our computations. Numerical parameters are chosen in order to obtain five figure agreement between the left and right hand sides of (7.8). This was typically obtained for $\Delta x = (1/120)$ m.

8. Results

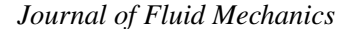
Throughout this results section, we take $H = 20 \,\mathrm{m}$ and $\rho h = 1 \,\mathrm{kg} \,\mathrm{m}^{-1}$. We consider three cases of the rigidity coefficients, as outlined in Table 1. We take the incident wave to be an incident plane wave of the form (7.1) with $A = 1 \,\mathrm{m}$ and $\chi = 0$ (i.e., it is travelling in the positive x direction) unless otherwise stated. The time averaged kinetic energy of the plate is

$$\bar{E}_{kin} = \frac{\rho h \omega^2}{4} \int_0^a \int_0^b |w(x, y)|^2 dy dx = \frac{\rho h \omega^2}{4} \sum_{j=1}^\infty |c_j|^2.$$
 (8.1)

This quantity is used to identify resonant frequencies of the plate.

Figure 3 shows the kinetic energy spectrum for a square isotropic plate. The two peaks correspond to resonances of the plate, which we investigate in Figures 4 and 5. We observe that the first resonance is predominantly associated with excitation of the first mode of vibration of the plate, whereas the second resonance is predominantly associated with excitation of the second and third modes in equal amounts. This is unsurprising because the second and third modes are degenerate, as shown in Figure 2. We note that in both cases, the fourth mode of the plate is not excited (i.e., $c_4 = 0$) because it is antisymmetric with respect to the line y = b/2, while the incident wave is symmetric with respect to this line. We remark that the far field patterns (Figure 4b and d) are symmetric with respect to $\theta = 0$, and the surface elevations (Figure 5) are symmetric about y = b/2.

Next, we consider a square orthotropic plate. The kinetic energy spectrum in Figure 6 again has two peaks, which we investigate in Figures 7 and 8. The first resonance is predominantly associated with excitation of the first plate mode, whereas the second



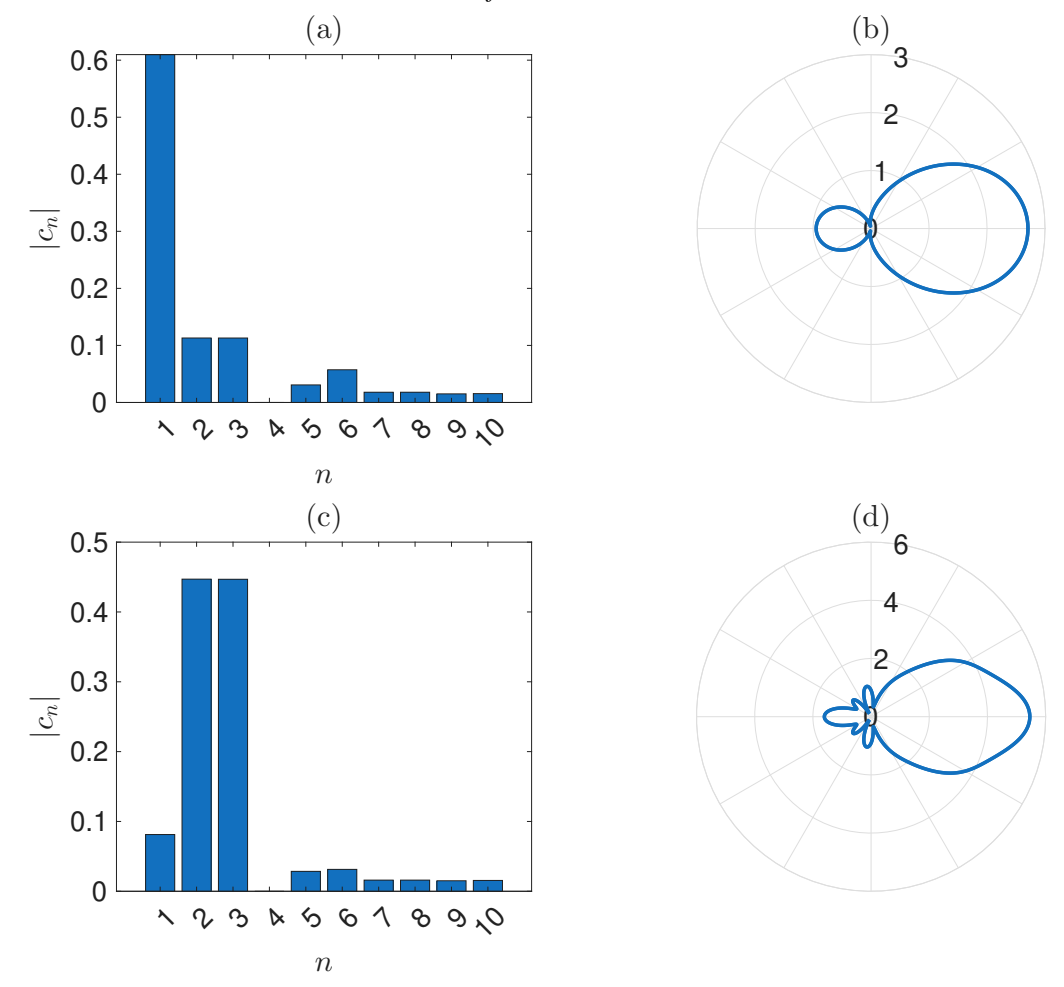


Figure 4. Mode expansion coefficient magnitudes (left column) and far field patterns (i.e., polar plots of $f(\theta)$, right column) at resonant frequencies of the square isotropic plate with a = b = 1 m. In particular, the nondimensionalised wavenumbers associated with the resonant frequencies are (a,b) ka = 4.23 and (c,d) ka = 10.44.

resonance is predominantly associated with excitation of the third plate mode. In contrast with the square isotropic plate considered earlier, the second and third modes of the orthotropic plate are not degenerate because symmetry has been broken. In particular, the second mode of the orthotropic plate is antisymmetric with respect to the line y = b/2 and hence cannot be excited by the symmetric incident plane wave. This also remains the case with the fourth mode. Thus we observe $c_2 = c_4 = 0$ in Figure 7. We remark that the far field patterns (Figure 7b and d) are symmetric with respect to $\theta = 0$, and the surface elevations (Figure 8) are symmetric about y = b/2.

The next case we consider is a square anisotropic plate, as parametrised by An *et al.* (2021). These parameters, which are reproduced in Table 1, describe a graphite/epoxy laminated plate in which the tensor describing the material is rotated by 45° in the *xy*-plane. As such, the modes of vibration in Figure 2 are symmetric or antisymmetric with respect to the lines y = x and x + y = a. The response of the surface-mounted square anisotropic plate to a plane wave with incident angle $\chi = 0$ is considered in Figures 9–11.

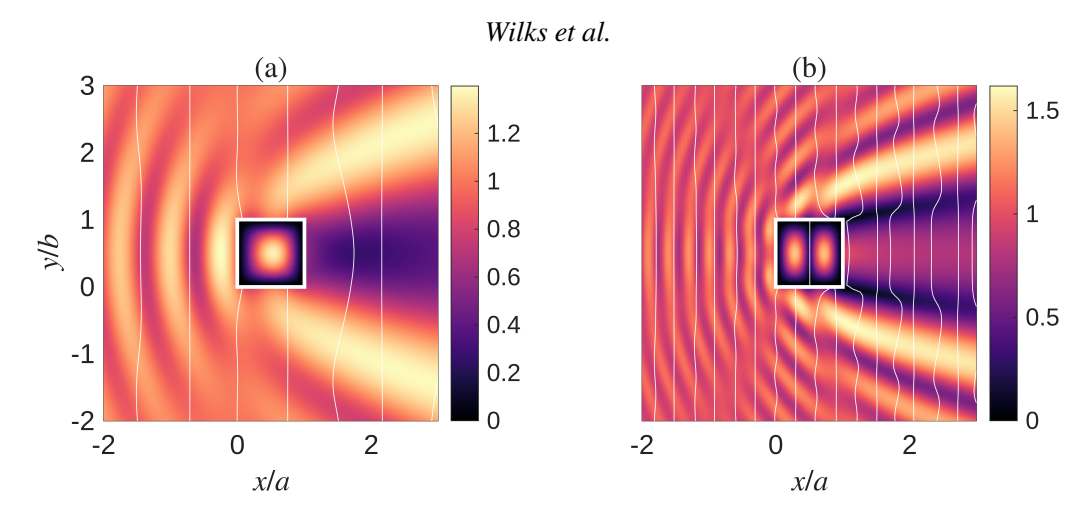


Figure 5. Surface elevation of the excited square isotropic plate (a = b = 1 m) at the resonant frequencies considered in Figure 4, namely (a) ka = 4.23 and (b) ka = 10.44. The surface elevation refers to |w| over the plate, and $|\eta|$ otherwise. The absolute value of the surface elevation is indicated by the colour scale, with white isophasic contours indicating where the surface elevation is real. The boundary of the plate is marked with a thick white line.

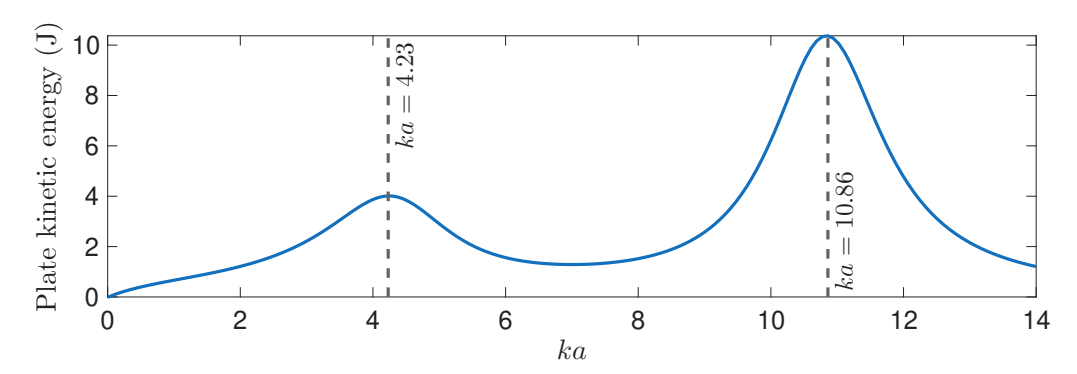


Figure 6. Kinetic energy spectrum for a square orthotropic plate, with a = b = 1 m.

We observe three resonant peaks in the kinetic energy spectrum (Figure 9), which are predominantly associated with excitation of the first three modes of vibration in order of increasing frequency. The second and third modes of vibration are not degenerate, and neither are antisymmetric with respect to the line y = b/2, so both can be excited. We remark that the far field patterns (Figure 10b, d and f) and the surface elevations (Figure 11) do not possess any symmetry. Observe that while Figures 10b and 11a may appear at first glance to suggest a symmetric response, this is due to the first mode shape (Figure 2i) being close to symmetric—there are in fact subtle asymmetries in Figure 11.

Figures 12–14 also explore the square anisotropic plate, although this time the angle of the incident wave is modified to $\chi = \pi/4$. This incident wave is symmetric with respect to the line y = x, so modes that are antisymmetric with respect to this line should not resonate. Indeed, we observe that $c_2 = 0$, meaning that the second mode of vibration is not excited because it does have this antisymmetry (see Figure 2). Moreover, there is no peak around ka = 10.11 in the kinetic energy spectrum—this peak having been associated with excitation of the second mode in the $\chi = 0$ case. We remark that the far field patterns (Figure 13b and d) are symmetric with respect to $\theta = \pi/4$, and the surface elevations (Figure 14) are symmetric about the line y = x.

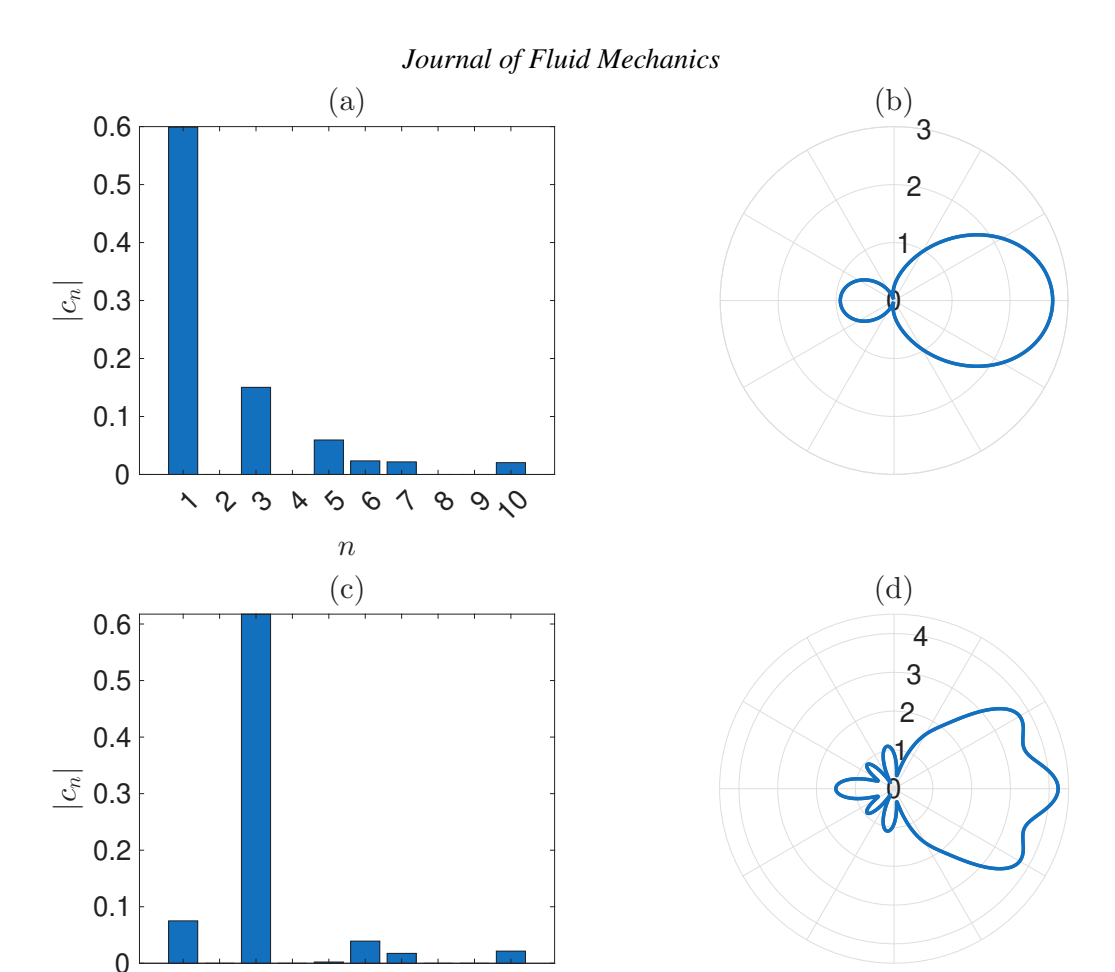


Figure 7. Mode expansion coefficient magnitudes (left column) and far field patterns (right column) at resonant frequencies of the square orthotropic plate with a = b = 1 m. The nondimensionalised wavenumbers are (a,b) ka = 4.23 and (c,d) ka = 10.86.

n

Lastly, we present results for rectangular plates, with $a=2\,\mathrm{m}$ and $b=1\,\mathrm{m}$, considering both the orthotropic and anisotropic cases. The first four mode shapes of both cases are given in Figure 15. Their kinetic energy spectra are given in Figures 16 and 19, each having three resonant peaks in the frequency interval considered. The relative excitations of the various plate modes at these resonant frequencies are given in Figure 17 for the orthotropic case, and Figure 20 for the anisotropic case. In both cases, we do not observe a strong resonant peak associated with the first plate mode. Moreover, in the orthotropic case, the fourth resonant mode is never excited because it is antisymmetric with respect to y=b/2, whereas the incident wave is symmetric with respect to this line. Finally, surface elevations of the first three resonances of orthotropic and anisotropic plates are given in Figures 18 and 21, respectively.

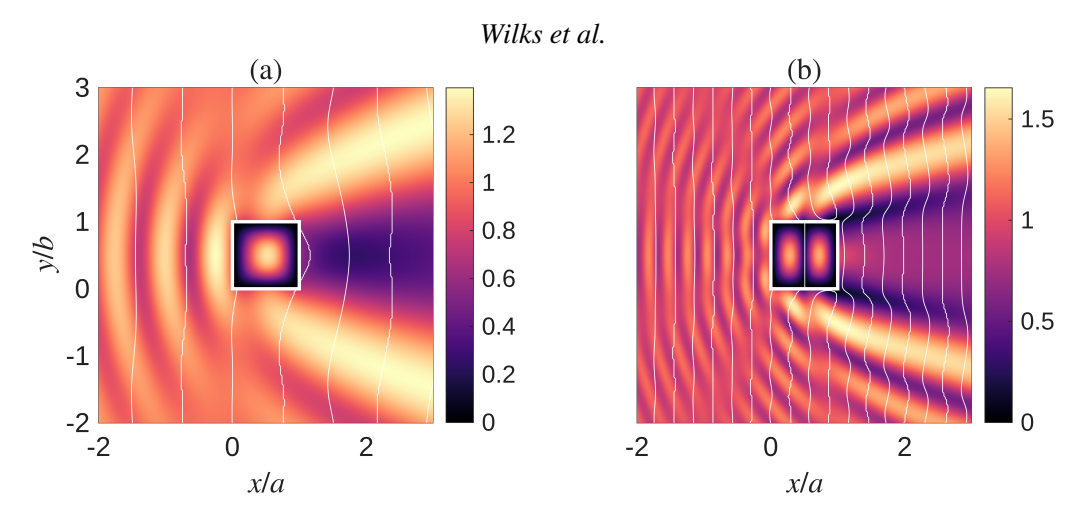


Figure 8. Surface elevation of the excited square orthotropic plate (a = b = 1 m) at the resonant frequencies considered in Figure 7, namely (a) ka = 4.23 and (b) ka = 10.86.

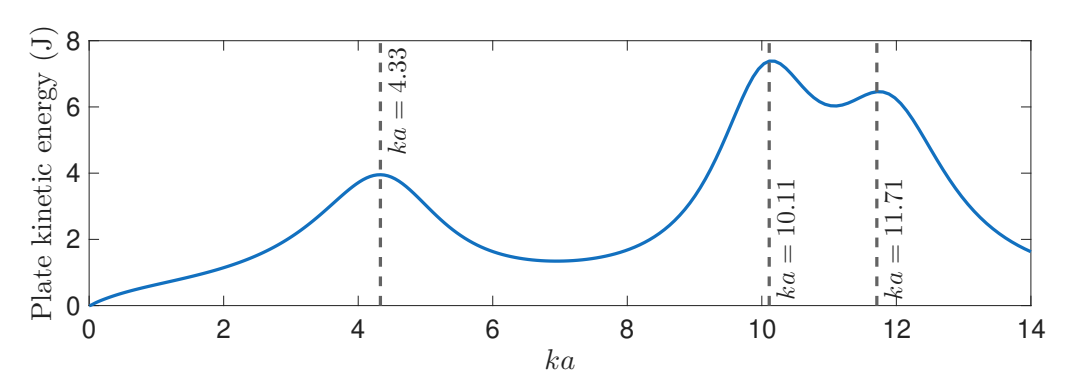


Figure 9. Kinetic energy spectrum for a square anisotropic plate, with a = b = 1 m.

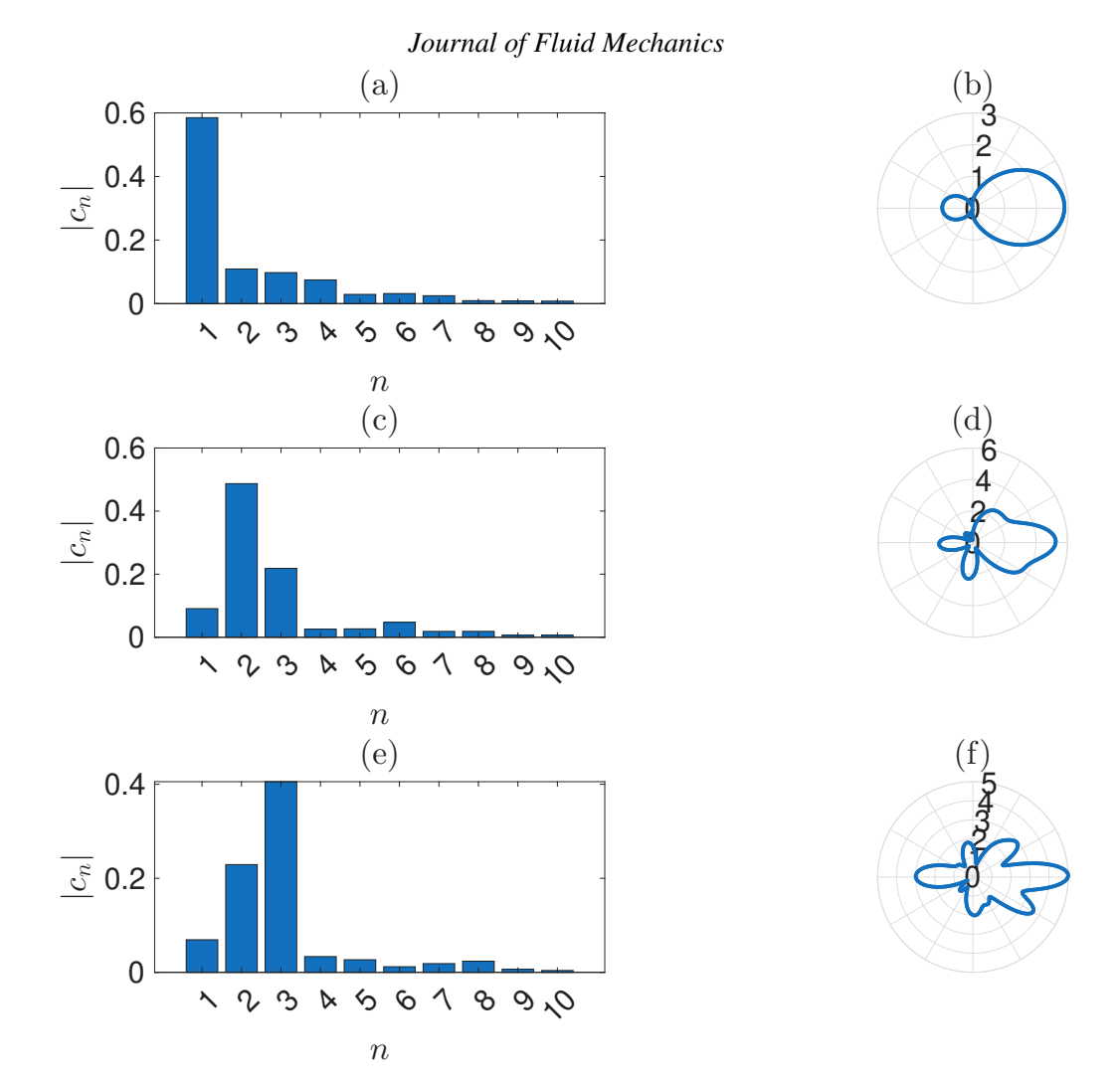


Figure 10. Mode expansion coefficient magnitudes (left column) and far field patterns (right column) at resonant frequencies of the square anisotropic plate with a = b = 1 m. The nondimensionalised wavenumbers are (a,b) ka = 4.33, (c,d) ka = 10.11 and (e,f) ka = 11.71.

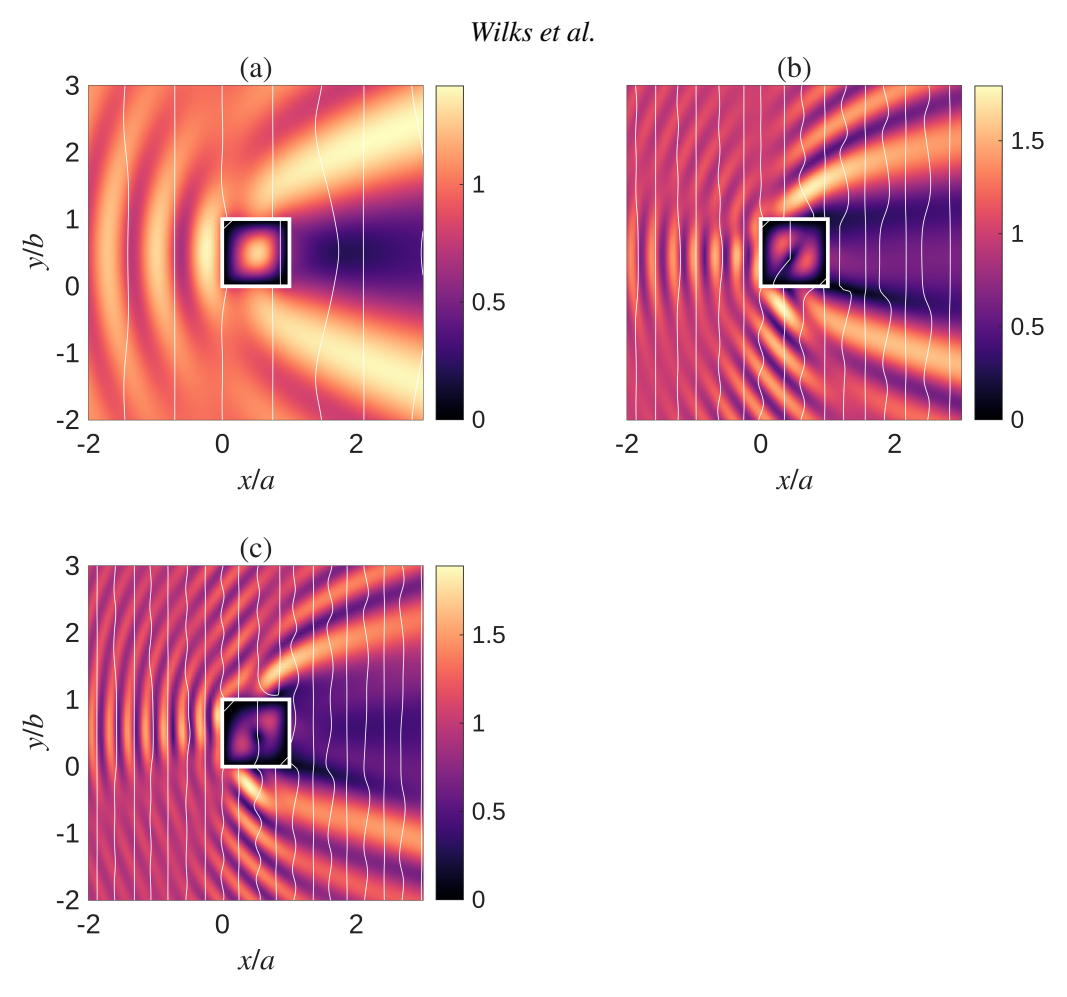


Figure 11. Surface elevation of the excited square isotropic plate (a = b = 1 m) at the resonant frequencies considered in Figure 10, namely (a) ka = 4.18, (b) ka = 10.11 and (c) ka = 11.71.

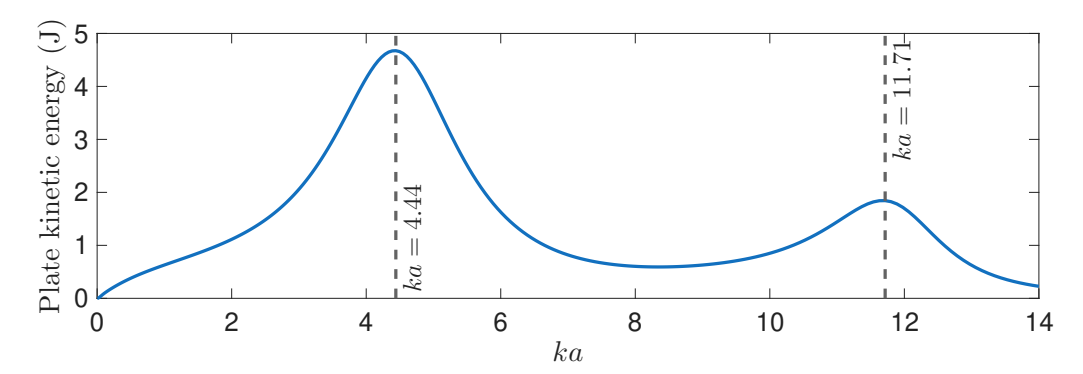
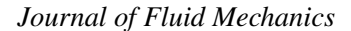


Figure 12. Kinetic energy spectrum for a square anisotropic plate, with a = b = 1 m (as in Figure 9) and with the direction of the incident wave being $\pi/4$.



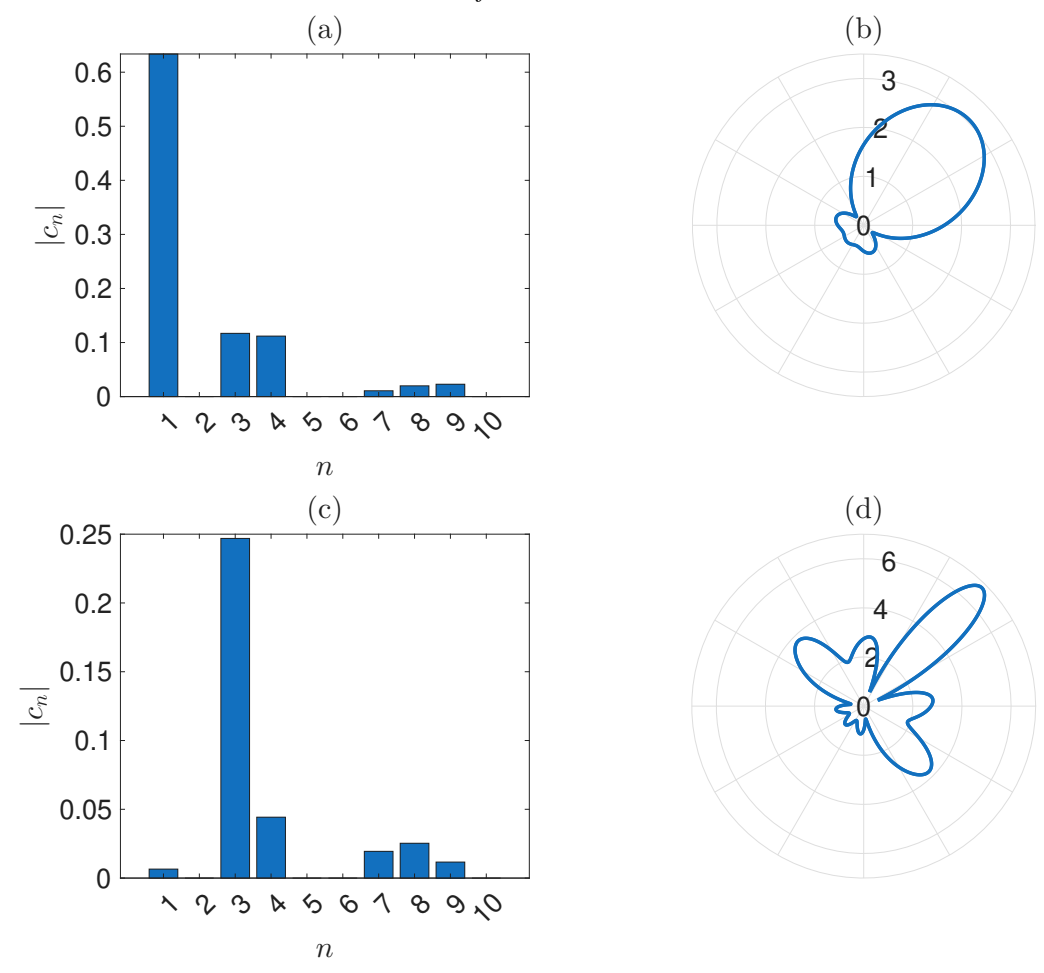


Figure 13. Mode expansion coefficient magnitudes (left column) and far field patterns (right column) at resonant frequencies of the square anisotropic plate with $a=b=1\,\mathrm{m}$, with the incident angle $\pi/4$. The nondimensionalised wavenumbers are (a) ka=4.44 and (b) ka=11.71.

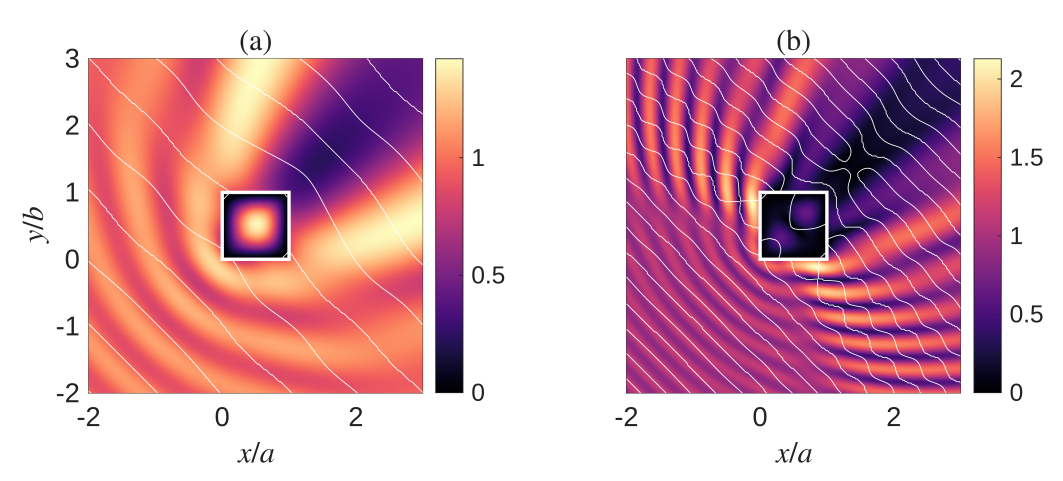


Figure 14. Surface elevation of the excited square isotropic plate (a = b = 1 m) with incident angle $\pi/4$ at the resonant frequencies considered in Figure 13, namely (a) ka = 4.4404 and (b) ka = 11.7144.

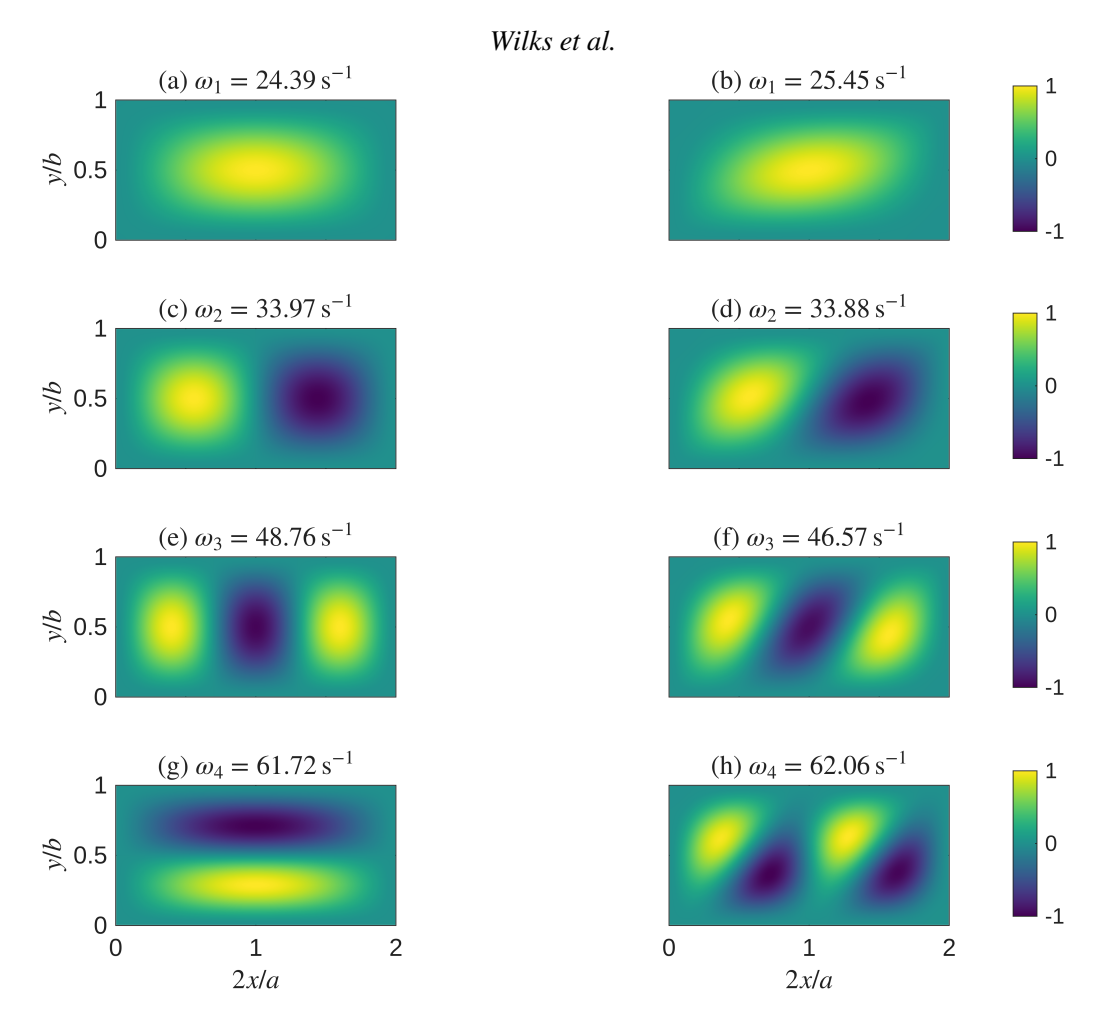


Figure 15. First four mode shapes of an (a,c,e,g) orthotropic and (b,d,f,h) anisotropic rectangular plate, with a=2 m and b=1 m.

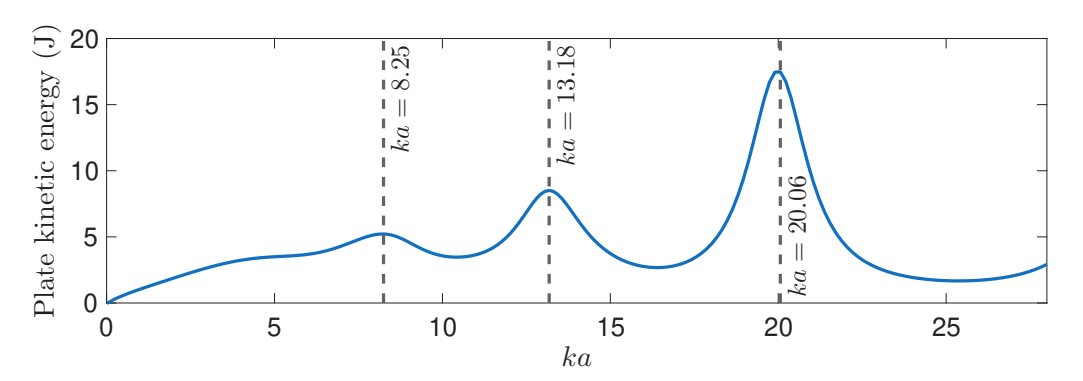


Figure 16. Kinetic energy spectrum for a rectangular orthotropic plate, with $a = 2 \,\mathrm{m}$ and $b = 1 \,\mathrm{m}$.

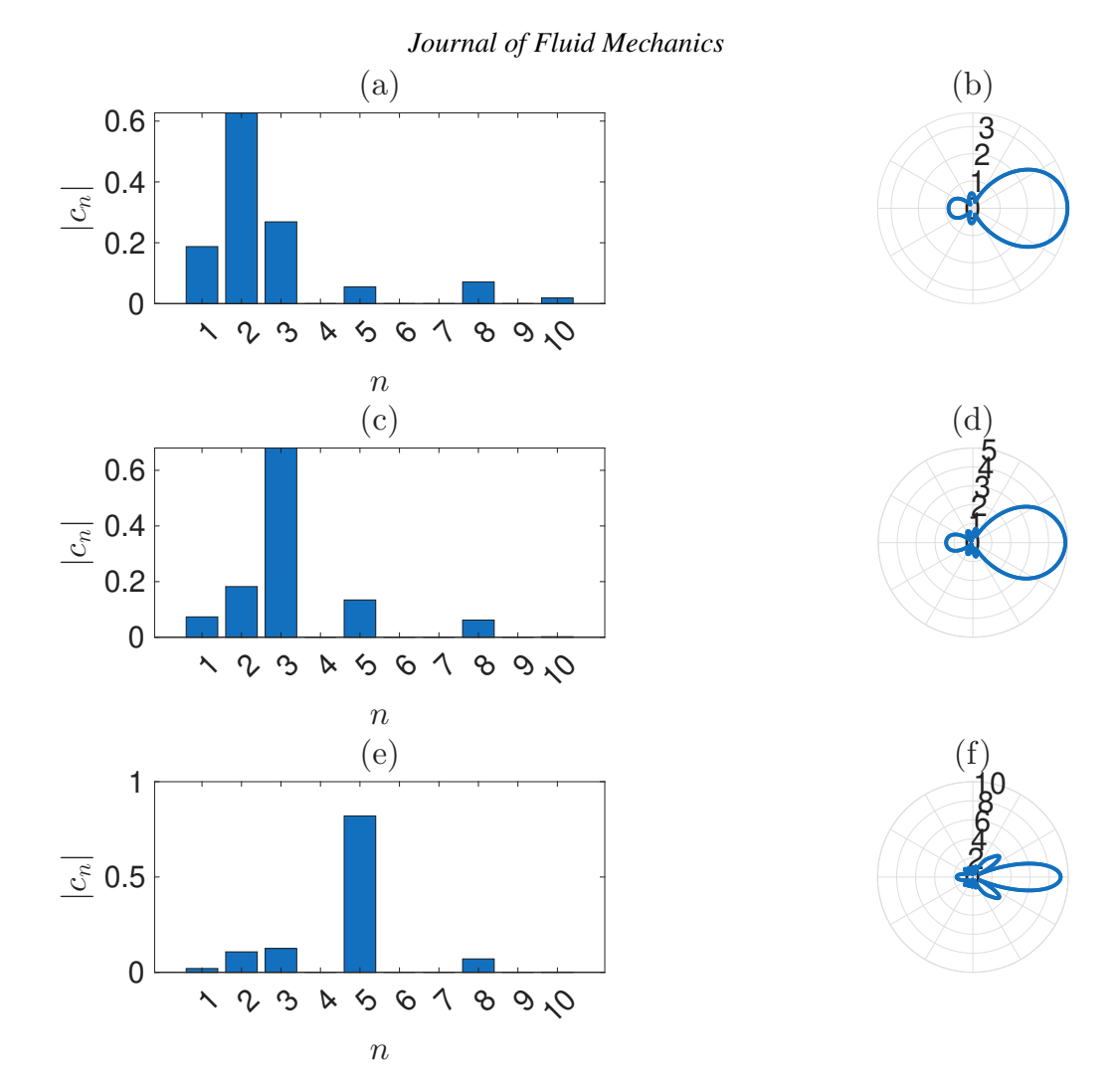


Figure 17. Mode expansion coefficient magnitudes (left column) and far field patterns (right column) at resonant frequencies of the rectangular orthotropic plate with a = 2 m and b = 1 m. The nondimensionalised wavenumbers are (a,b) ka = 8.25, (c,d) ka = 13.18 and (e,f) ka = 20.06.

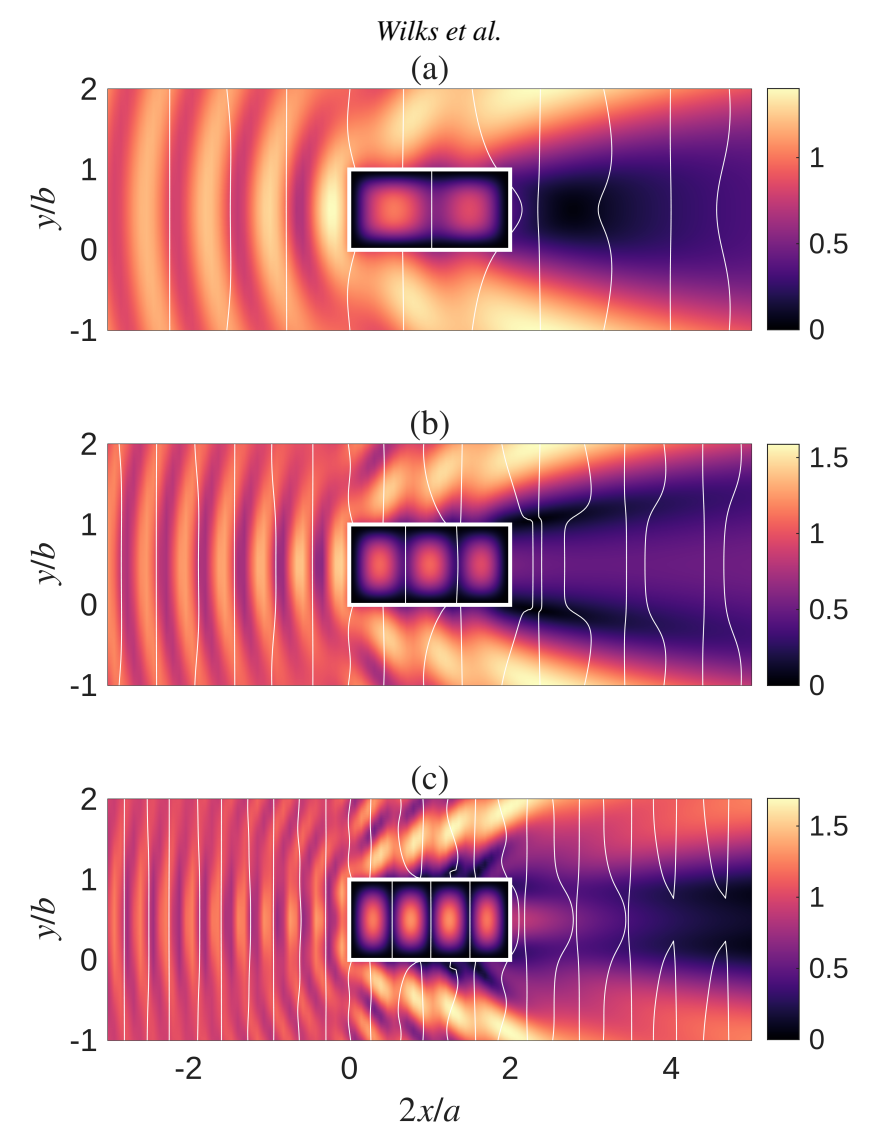


Figure 18. Surface elevation of the excited rectangular orthotropic plate (a = 2 m and b = 1 m) at the resonant frequencies considered in Figure 17, namely (a) ka = 8.25, (b) ka = 13.18 and (c) ka = 20.06.

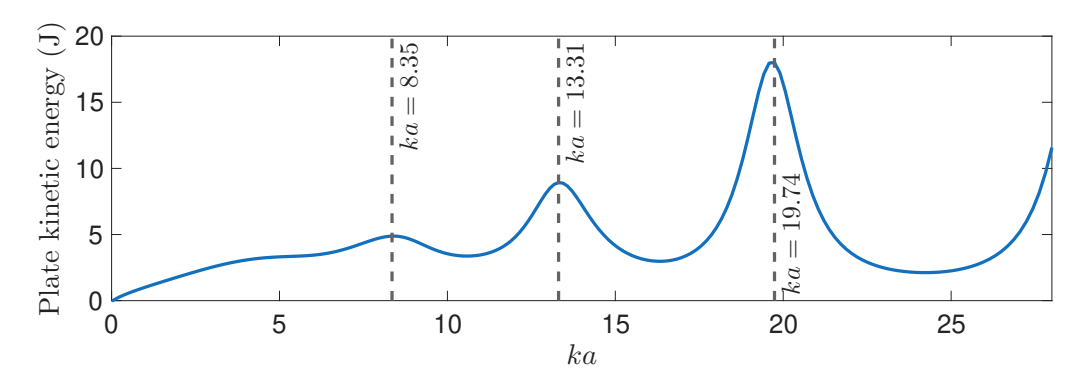


Figure 19. Kinetic energy spectrum for a rectangular anisotropic plate, with $a = 2 \,\mathrm{m}$ and $b = 1 \,\mathrm{m}$.

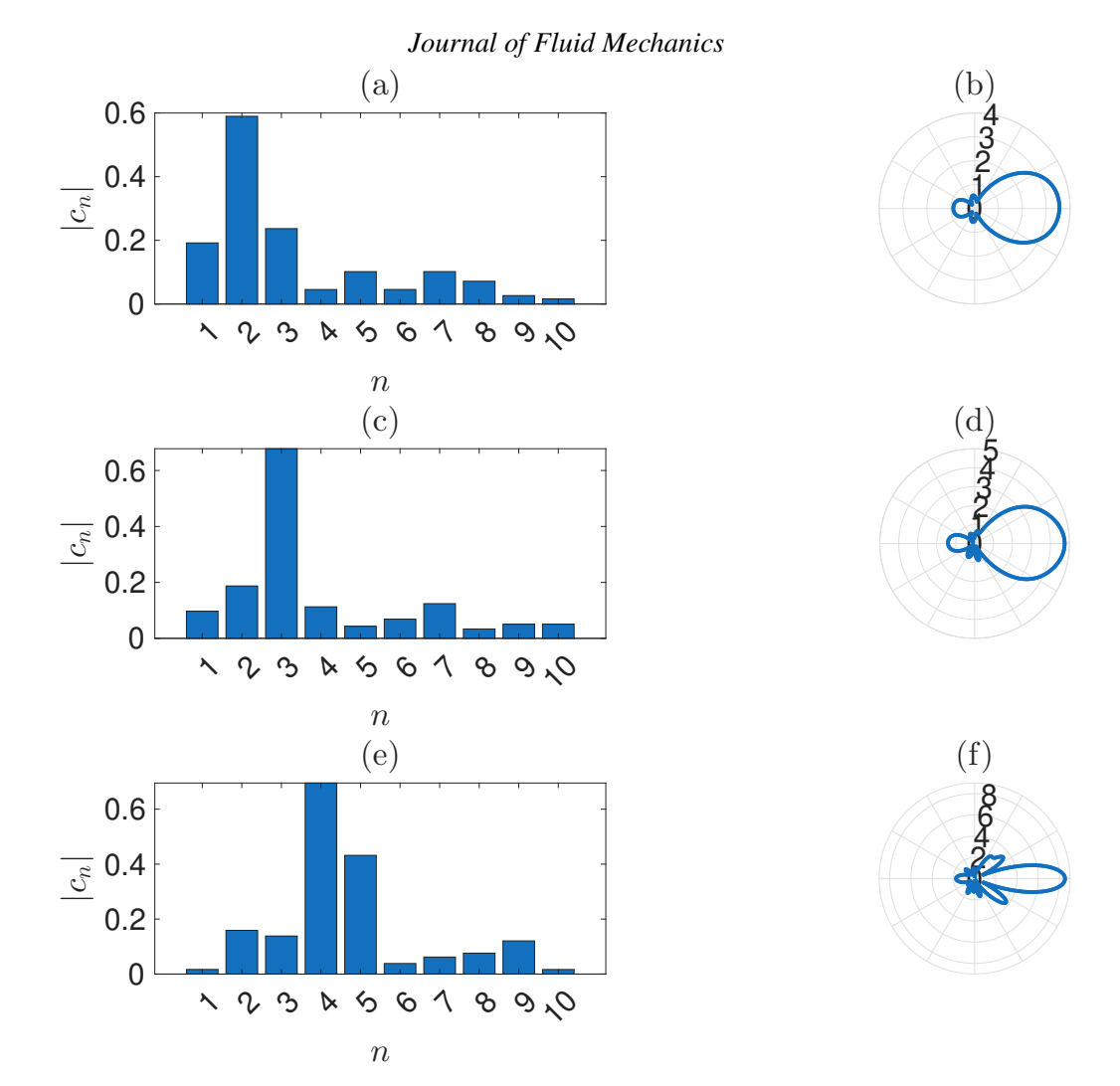


Figure 20. Mode expansion coefficient magnitudes (left column) and far field patterns (right column) at resonant frequencies of the rectangular anisotropic plate with a = 2 m and b = 1 m. The nondimensionalised wavenumbers are (a,b) ka = 8.35, (c,d) ka = 13.31 and (e,f) ka = 19.74.

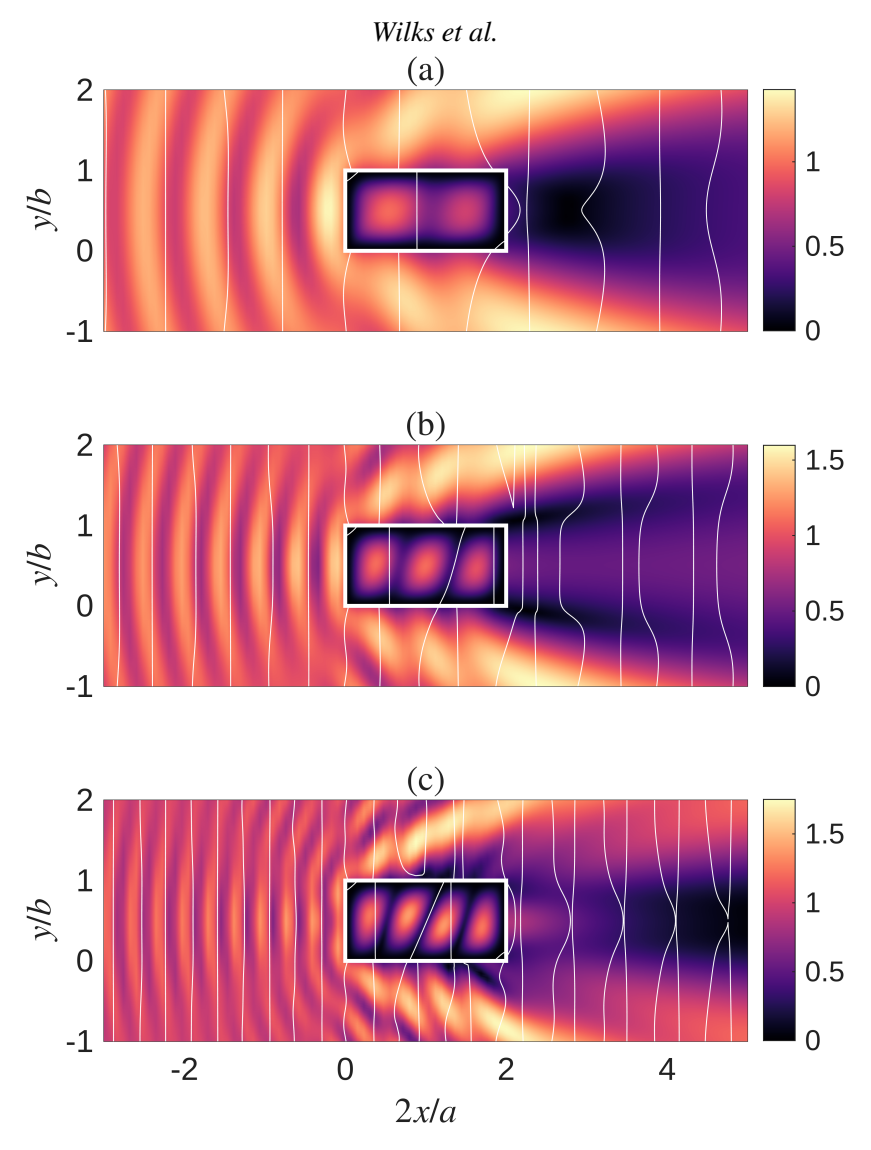


Figure 21. Surface elevation of the excited rectangular anisotropic plate (a = 2 m and b = 1 m) at the resonant frequencies considered in Figure 20, namely (a) ka = 8.35, (b) ka = 13.31 and (c) ka = 19.74.

Journal of Fluid Mechanics

9. Conclusion

This paper has considered the problem of water wave scattering by a surface mounted rectangular anisotropic elastic plate, with clamped boundaries. Other boundary types (e.g., simply supported or free boundaries) could easily be considered within the present formulation, but this is left as an area of future work. The problem was solved by expanding in the modes of vibration of the plate, with the required diffraction and radiation problems being solved using a boundary integral equation/constant panel method. Results for isotropic, orthotropic and anisotropic plates of either square or rectangular geometries were presented that illustrate the capabilities of the numerical method. Overall, our results show that the response by the plate can depend greatly on the rigidity coefficients D_{ij} . Our investigation has emphasised that the excitation of certain modes can be forbidden if they are symmetrically opposed to the incident wave.

The main motivation of this work was an application to the modelling of PWECs, and this remains as an area of future work. The method presented here can be used (essentially verbatim) for a surface mounted rectangular piezoelectric plate, with the rigidity coefficients D_{ij} becoming complex. The only necessary adjustment resulting from this would be to the modal expansion method presented in §6, because the set of plate eigenmodes w_j will no longer be orthogonal in general. We stress that our approach will allow the anisotropy of the piezoelectric material within the WEC to be modelled appropriately in three dimensions. Another possible extension of this work is to arbitrary shaped plates, as considered by Meylan (2002) for isotropic plates with free edges. Although the modes of vibration would need be calculated using a different method to the one presented in §4 (e.g., the finite element method could be used), the hydrodynamic component of the solution could remain unchanged. Lastly, we mention the problem of extending this study to submerged horizontal plates. This case is more complicated from a mathematical perspective because it leads to hypersingular integral equations.

Funding

This study was supported by the Australian Research Council's Discovery Projects funding scheme (DP240102104).

Declaration of Interests

The authors report no conflict of interest.

Data availability

Data sharing does not apply to this article, as no new data was created or analysed in this study. The computer code used to generate the solutions is available from the corresponding author upon reasonable request.

Appendix A. Beam eigenfunctions

The solutions of the eigenfunction problem (4.3) may be expressed as

$$u(x) = a_1 \sin(\kappa x) + a_2 \cos(\kappa x) + a_3 e^{-\kappa x} + a_4 e^{\kappa(x-1)}.$$
 (A1)

In order for the boundary conditions to be satisfied, we must find κ for which the following nullspace problem has a nontrivial solution

$$\begin{bmatrix} 0 & 1 & 1 & e^{-\kappa} \\ \sin(\kappa) & \cos(\kappa) & e^{-\kappa} & 1 \\ 1 & 0 & -1 & e^{-\kappa} \\ \cos(\kappa) & -\sin(\kappa) & -e^{-\kappa} & 1 \end{bmatrix} \begin{bmatrix} a_1 \\ a_2 \\ a_3 \\ a_4 \end{bmatrix} = \begin{bmatrix} 0 \\ 0 \\ 0 \\ 0 \end{bmatrix}.$$
 (A 2)

This is true when the determinant of the matrix is zero, which can be shown to occur when

$$\operatorname{sech}(\kappa) = \cos(\kappa).$$
 (A3)

We remark that the tasks of normalising of the eigenfunctions u_m in accordance with (4.4), and computing the quantities $\mathcal{U}_{mp}^{[l]}$ introduced in (4.7), require the computation of integrals that would be tedious to calculate by hand. Instead, symbolic computation was used to obtain suitable expressions, which were then verified by numerical integration.

REFERENCES

- An, Dongqi, Ni, Zhuofan, Xu, Dian & Li, Rui 2021 New straightforward benchmark solutions for bending and free vibration of clamped anisotropic rectangular thin plates. *Journal of Vibration and Acoustics* **144** (3), 031011
- Andrianov, Alexey I & Hermans, And J 2006 Hydroelastic behavior of a floating ring-shaped plate. *Journal of Engineering Mathematics* **54** (1), 31–48.
- Babarit, Aurélien, Singh, Jitendra, Mélis, Cécile, Wattez, Ambroise & Jean, Philippe 2017 A linear numerical model for analysing the hydroelastic response of a flexible electroactive wave energy converter. *Journal of Fluids and Structures* 74, 356–384.
- Balmforth, N J & Craster, R V 1999 Ocean waves and ice sheets. *Journal of Fluid Mechanics* **395**, 89–124. Cheng, Yong, Du, Weiming, Dai, Saishuai, Yuan, Zhiming & Incecik, Atilla 2024 Wave energy conversion by an array of oscillating water columns deployed along a long-flexible floating breakwater. *Renewable and Sustainable Energy Reviews* **192**, 114206.
- Chung, Hyuck & Fox, Colin 2002 Calculation of wave-ice interaction using the Wiener-Hopf technique. *New Zealand Journal of Mathematics* **31** (1), 1–18.
- Collins, Ieuan, Hossain, Mokarram, Dettmer, Wulf & Masters, Ian 2021 Flexible membrane structures for wave energy harvesting: A review of the developments, materials and computational modelling approaches. *Renewable and Sustainable Energy Reviews* **151**, 111478.
- FALNES, JOHANNES 2002 Ocean Waves and Oscillating Systems, 1st edn. Cambridge University Press.
- Fox, C. & SQUIRE, V. A. 1994 On the oblique reflexion and transmission of ocean waves at shore fast sea ice. *Philosophical Transactions of the Royal Society of London. Series A* **347** (1682), 185–218.
- Guo, Yu Chan, Mohapatra, SC & Soares, C Guedes 2023 An experimental study on the performance of combined membrane breakwaters against incident waves. *Ocean Engineering* **280**, 114793.
- HERMANS, A J 2004 Interaction of free-surface waves with floating flexible strips. *Journal of Engineering Mathematics* **49** (2), 133–147.
- Leissa, A.W. 1973 The free vibration of rectangular plates. Journal of Sound and Vibration 31 (3), 257–293.
- LINTON, C. M. & McIver, P. 2001 Handbook of mathematical techniques for wave/structure interactions. Chapman & Hall.
- MEI, CHIANG C., STIASSNIE, MICHAEL & YUE, DICK K. P. 2005 Theory and applications of ocean surface waves Part 1: Linear aspects. World Scientific.
- MEYLAN, M. H. 2001 A variation equation for the wave forcing of floating thin plates. *Applied Ocean Research* **23** (4), 195–206.
- MEYLAN, MICHAEL H 2002 Wave response of an ice floe of arbitrary geometry. *Journal of Geophysical Research: Oceans* **107** (C1), 5–1.
- MEYLAN, MICHAEL H., CHALLIS, VIVIEN J., THAMWATTANA, NGAMTA, WEGERT, ZACHARY J. & WILKS, BEN 2025 Wave power absorption by floating plates with application to piezoelectric or other bending-based absorption. *Ocean Engineering* **328**, 120931.
- MEYLAN, M. H. & SQUIRE, V. A. 1994 The response of ice floes to ocean waves. *Journal of Geophysical Research: Oceans* **99** (C1), 891–900.
- MEYLAN, M. H. & SQUIRE, V. A. 1996 Response of a circular ice floe to ocean waves. *Journal of Geophysical Research: Oceans* **101** (C4), 8869–8884.
- MICHELE, SIMONE, ZHENG, SIMING & GREAVES, DEBORAH 2022 Wave energy extraction from a floating flexible circular plate. *Ocean Engineering* **245**, 110275.
- NEWMAN, JOHN NICHOLAS 1994 Wave effects on deformable bodies. Applied Ocean Research 16 (1), 47–59.
- Peter, M. A., Meylan, M. H. & Chung, H. 2004 Wave scattering by a circular elastic plate in water of finite depth: a closed form solution. *International Journal of Offshore and Polar Engineering* 14 (2), 81–85.
- Philen, Michael, Squibb, Carson, Groo, LoriAnne & Hagerman, George 2018 Wave energy conversion using fluidic flexible matrix composite power take-off pumps. *Energy Conversion and Management* 171, 1773–1786.
- RENZI, E. 2016 Hydroelectromechanical modelling of a piezoelectric wave energy converter. Proceedings of the Royal Society A 472 (2195), 20160715.

Journal of Fluid Mechanics

- Renzi, Emiliano, Michele, Simone, Zheng, Siming, Jin, Siya & Greaves, Deborah 2021 Niche applications and flexible devices for wave energy conversion: A review. *Energies* 14 (20), 6537.
- Sahoo, T, Yip, Tsz Leung & Chwang, Allen T 2001 Scattering of surface waves by a semi-infinite floating elastic plate. *Physics of Fluids* **13** (11), 3215–3222.
- SINGH, MANSI & GAYEN, R 2023 Performance of two vertically submerged piezoelectric plate wave energy converters in presence of a non-flat flexible barrier. *Renewable Energy* **212**, 382–393.
- SMITH, M J A, PETER, MALTE A, ABRAHAMS, I D & MEYLAN, M H 2020 On the Wiener-Hopf solution of water-wave interaction with a submerged elastic or poroelastic plate. *Proceedings of the Royal Society A: Mathematical, Physical and Engineering Sciences* 476 (2242), 20200360.
- Squire, V A 2007 Of ocean waves and sea-ice revisited. *Cold Regions Science and Technology* **49** (2), 110–133. Squire, V. A. 2020 Ocean wave interactions with sea ice: a reappraisal. *Annual Review of Fluid Mechanics* **52** (1), 37–60.
- Tay, Zhi Yung & Wei, Yanji 2020 Power enhancement of pontoon-type wave energy convertor via hydroelastic response and variable power take-off system. *Journal of Ocean Engineering and Science* 5 (1), 1–18.
- TKACHEVA, L A 2003 Plane problem of surface wave diffraction on a floating elastic plate. *Fluid Dynamics* **38** (3), 465–481.
- V., Vipin & Koley, Santanu 2022 Mathematical modeling of a submerged piezoelectric wave energy converter device installed over an undulated seabed. *Renewable Energy* 200, 1382–1392.
- VINOGRADOV, ALEKSANDRA & HOLLOWAY, FRANK 1999 Electro-mechanical properties of the piezoelectric polymer pvdf. Ferroelectrics 226 (1), 169–181.
- Wilks, Ben, Meylan, Michael H., Montiel, Fabien, Balasooriya, Dasun Shalila, Jauhar, Tahir, Wheeler, Craig & Chalup, Stephan 2025 Simultaneous layout and device parameter optimisation of a wave energy park in an irregular sea. *arXiv* preprint *arXiv*:2504.07122.
- WILLIAMS, T D & MEYLAN, MICHAEL H 2012 The Wiener-Hopf and residue calculus solutions for a submerged semi-infinite elastic plate. *Journal of Engineering Mathematics* **75** (1), 81–106.
- YANG, JIASHI 2018 An introduction to the theory of piezoelectricity, 2nd edn., Advances in Mechanics and Mathematics, vol. 9. Cham, Switzerland: Springer.
- ZHENG, SIMING, MICHELE, SIMONE, LIANG, HUI, MEYLAN, MICHAEL H & GREAVES, DEBORAH 2022 Wave power extraction from a floating elastic disk-shaped wave energy converter. *Journal of Fluid Mechanics* **948**, A38.